Biointerface Research in Applied Chemistry
Platinum Open Access Journal (ISSN: 2069-5837)

Article
Volume 12, Issue 2, 2022, 1651 - 1659
https://doi.org/10.33263/BRIAC122.16511659

Computational Investigating Fe-Doped Coronone Surface for Adsorption of Hydrogen Sulfide Gaseous Substance

Kun Harismah [1,*], Bahareh Zohrevand [2], Hasan Zandi [3]

[1] Department of Chemical Engineering, Faculty of Engineering, Universitas Muhammadiyah Surakarta, Surakarta, Indonesia; kun.harismah@ums.ac.id (K.H.);
[2] Department of Chemistry, Central Tehran Branch, Islamic Azad University, Tehran, Iran; bahar.zohrevand1994@gmail.com (B.Z.);
[3] Department of Chemistry, Faculty of Science, University of Qom, Qom, Iran; hasan_zandi@yahoo.com (H.Z.);
* Correspondence: kun.harismah@ums.ac.id (K.H.);

Scopus Author ID 56982926300

Received: 24.04.2021; Revised: 26.05.2021; Accepted: 28.05.2021; Published: 9.06.2021

Abstract: Hydrogen sulfide (H_2S) gas adsorption at the surface of iron (Fe)-doped model of coronene was investigated in this work by means of performing density functional theory (DFT) calculations. First, pure coronene and Fe-doped models were examined regarding the electronic and structural features. Next, different starting positions of H_2S molecule at the surface were examined during optimization processes yielded two conformational relaxations of H_2S-A and H_2S-B models. Various features of molecular and atomic scales were evaluated for the optimized modes to describe details of such adsorption processes, in which the results introduced the H_2S-A model more proper for the complex formation of H_2S and Fe-doped coronene. Interestingly, variations of molecular orbital levels could help diagnose opportunities for detecting the H_2S adsorbed model in addition to determining each of the A and B models. Consequently, a Fe-doped coronene surface could be proposed for proper adsorption of H_2S gaseous substance with removal and diagnosis purposes.

Keywords: coronene; hydrogen sulfide; gas adsorption; Fe-doped model; surface; DFT.

1. Introduction

Innovation of nanotechnology by pioneering work of Iijima in 1991 has raised considerable attempts to characterize the materials related to this novel technology besides exploring new functions [1-5]. Nanotechnology was initiated by carbon nanotubes (CNT), but several other types of nanostructures such as nanocone, nanocage, nanosheet, and nanoparticles with varieties of atomic compositions have been introduced by performing further investigations [6-10]. In addition to pure nanostructures, formations of atomic-doped models have been achieved useful for specified applications [11]. From the early days of nanotechnology, their roles in health-related fields have always been expected to solve more problems in these issues [12]. To this aim, several applications such as drug delivery and therapy have been examined for nanostructures in living systems besides exploring their exterior health applications such as gas adsorption for pollutant removal purposes [13-15]. Hydrogen sulfide (H_2S) is one of the most harmful gases available in the industrial environment, which should be removed regarding health care issues [16-18]. Besides poisoning function for living systems, it is a corrosive gas for destroying other materials making H_2S removal an important issue [19]. Therefore, considerable attempts have been dedicated to this

time for innovating surface materials for adsorption of H_2S gaseous substance removing from the environment [20-22]. The coronene surface was examined for adsorption of H2S gaseous substance within this work through performing quantum chemical calculations. Coronene is almost a single-standing molecular structure of graphene nanosheet to explore the advantage of applying such carbon-based nanosurface for substance adsorption processes [23-25]. As mentioned above about the importance of atomic doped nanostructures, the coronene of this work was doped by an iron atom to make a Fe-doped model for playing the role of nanosurface for adsorption of H_2S molecule (Figure 1). Earlier works indicated that such gaseous adsorption at nanosurface has indeed important details which should be clarified to reach a known process for such purpose [26-28]. Hence, H_2S adsorption at the Fe-doped coronene surface was investigated in this work using computer-based facilities to make sense of ideas as much as possible [29, 30]. As a clear notation, the main problem of this work was to computationally investigate the adsorption process of H_2S at the Fe-doped coronene surface to see the advantage of such nanostructure for this gaseous substance removal. To this aim, geometrical optimizations and molecular and atomic features evaluations were performed to provide the required information for discussing the problem of this work using Table 1 and Figures 1-5.

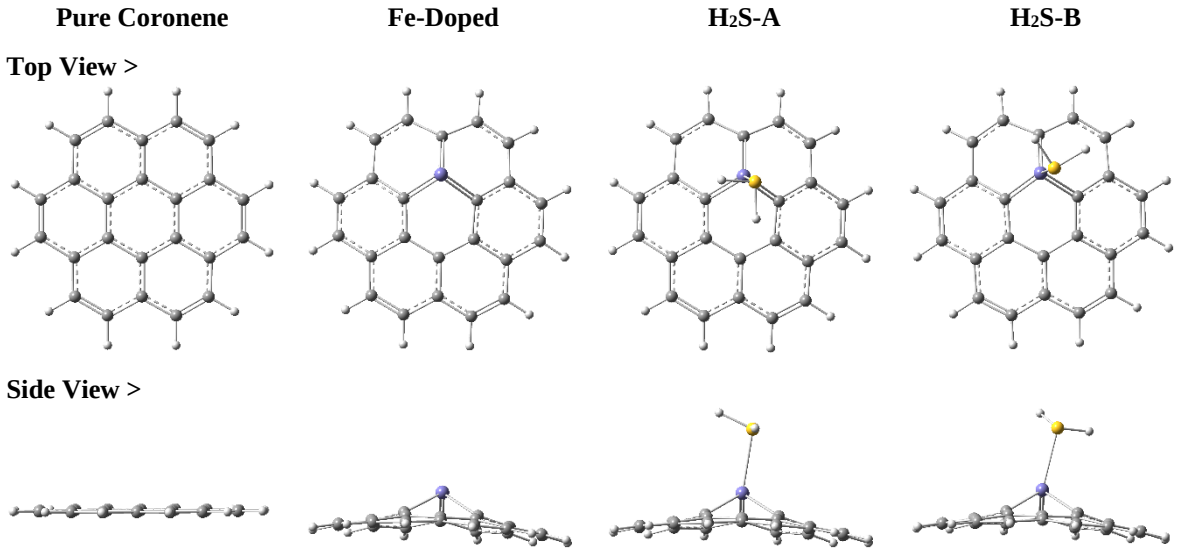

Figure 1. Views for the optimized models.

2. Materials and Methods

To prepare required nanosurface for H_2S adsorption, a 3D model of pure coronene ($C_{24}H_{12}$) was obtained from ChemSpider structural bank with ID 8761 [31]. The obtained structure was fully optimized first to reach the minimized energy structure, as indicated in Figure 1. Next, the Fe-doped model was created by substituting one iron atom instead of one carbon atom of a pure model. The Fe-doped model was fully optimized again to reach the minimized energy structure. A Fe-doped coronene surface was prepared for participating in adsorption of H2S gaseous substance by doing such processes. To carefully do such an adsorption process, all possible starting orientations of H_2S molecule versus the surface were examined to reach two conformational optimizations of H_2S at the Fe-doped surface designating by H_2S-A and H_2S-B models (Figure 1). Obtained bond distances for all the geometrically optimized models were exhibited in Figure 2. All structures' stability was confirmed by performing frequency calculations and providing infrared (IR) spectra (Figure 3).

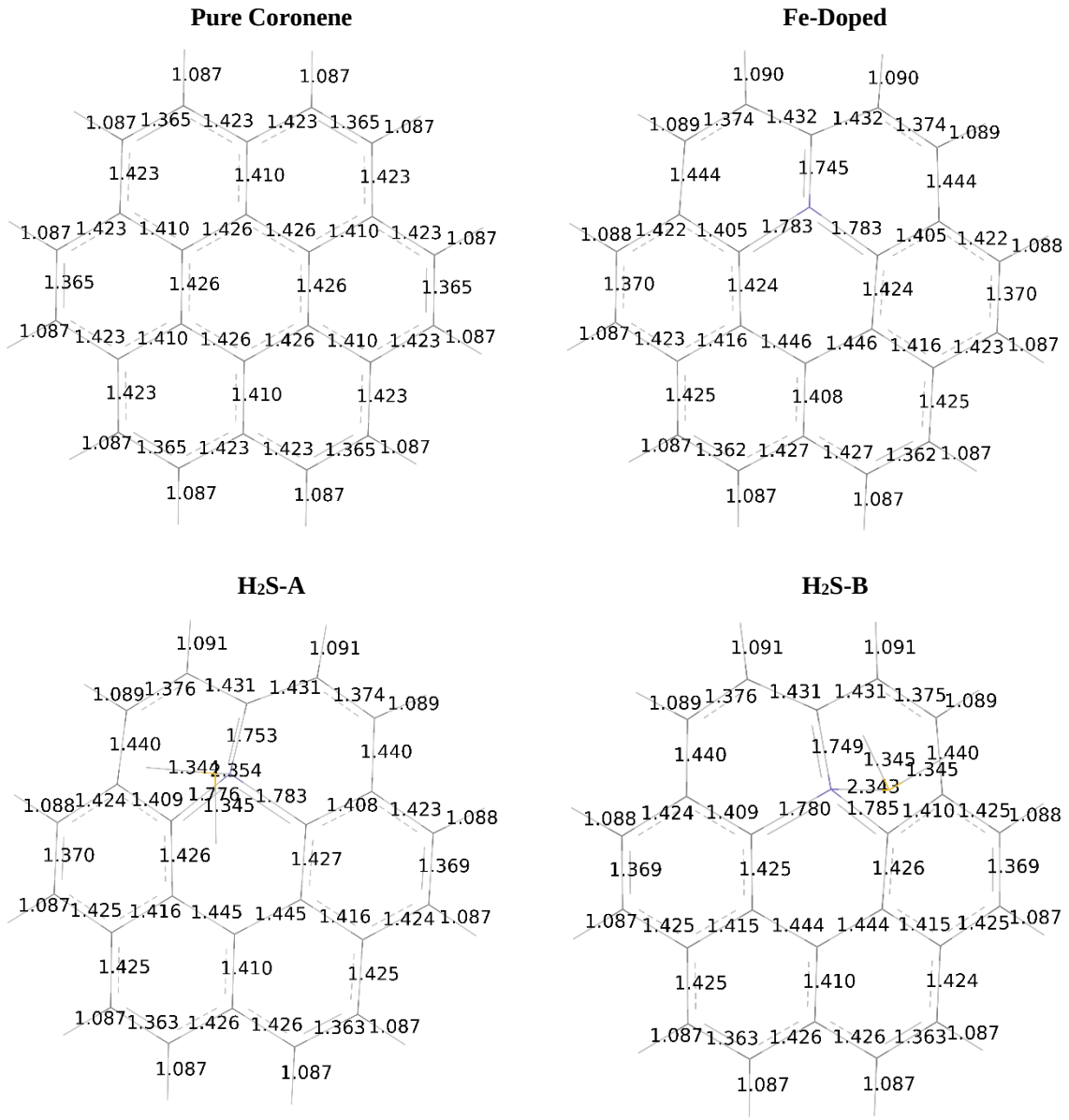

Figure 2. Bond lengths Å for the optimized models.

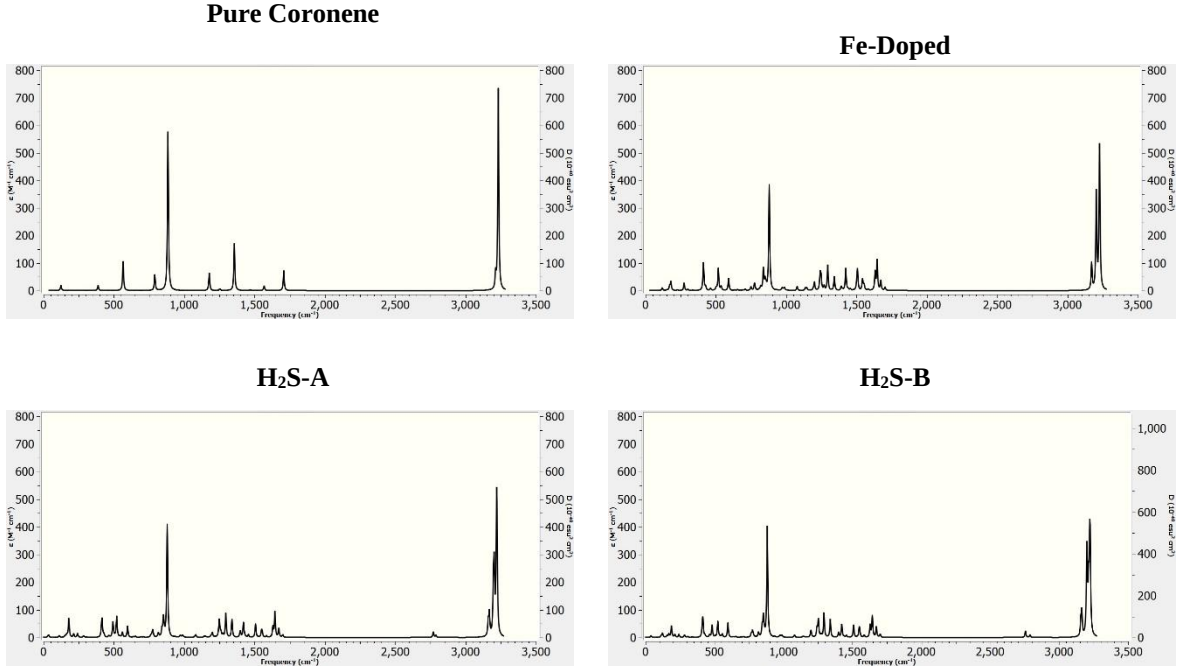

Figure 3. IR spectra for the optimized models.

Mulliken charge points were also evaluated for the optimized models, and they were exhibited in Figure 4. Furthermore, distribution patterns for the highest occupied and the lowest unoccupied molecular orbitals (HOMO and LUMO) and electrostatic potential (ESP) surfaces were represented in Figure 5. Besides such visual results, obtained quantities of energy (E), adsorption energy (Eads), basis set superposition error (BSSE), energy levels of HOMO and LUMO, energy gap (EG), Fermi energy (FE), dipole moment (DM), volume (V), and quadrupole coupling constant (Qcc) of the optimized models were all summarized in Table 1. To perform such computer-based work, the WB97XD/6-31g* level of density functional theory (DFT) was employed for calculations using the Gaussian program [32].

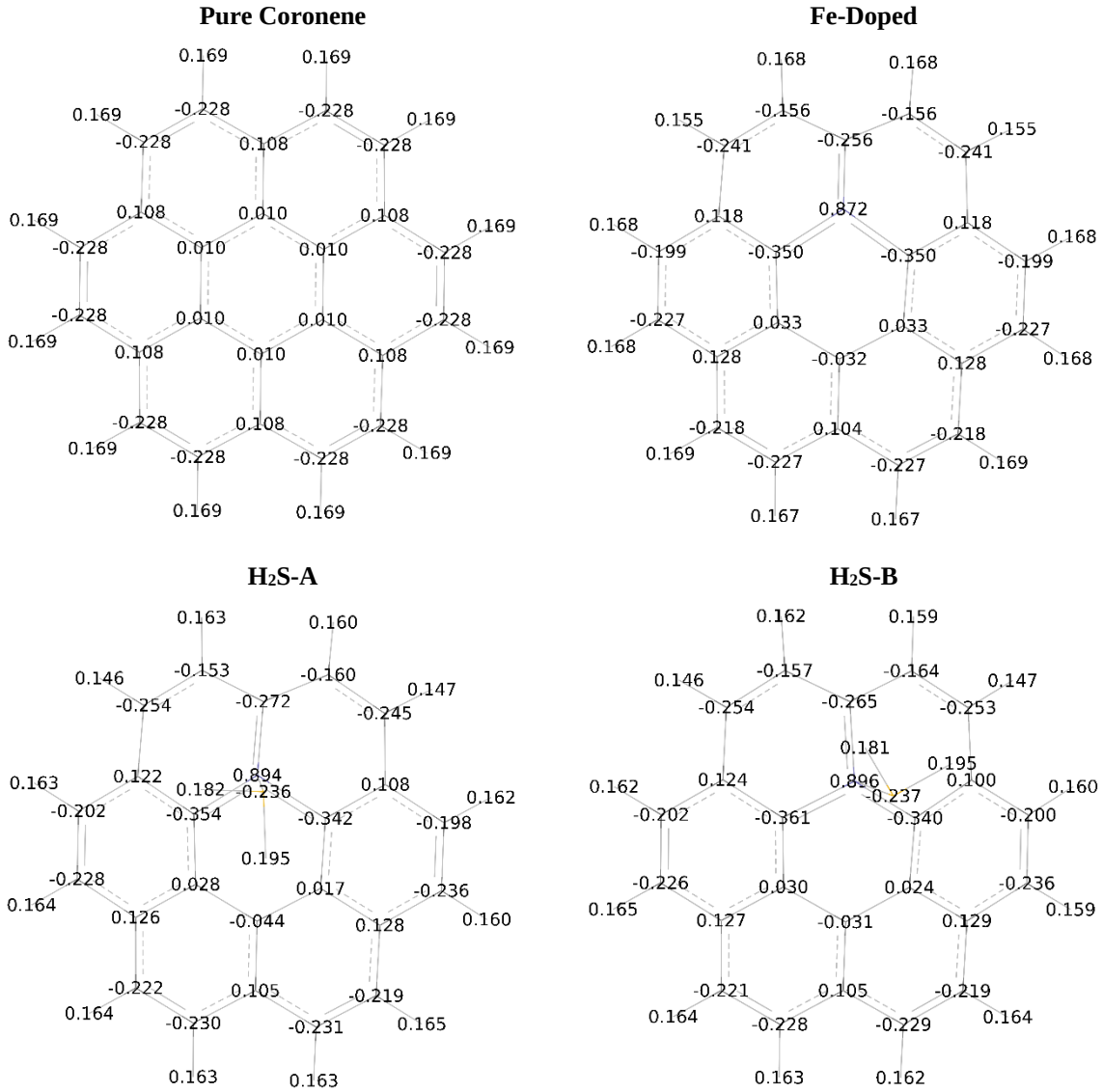

Figure 4. Mulliken charges for the optimized models.

3. Results and Discussion

H_2S gas adsorption at the surface of Fe-doped coronene was investigated in this work by means of DFT calculated results at the molecular and atomic scales (Table 1 and Figures 1-5). As exhibited in Figure 1, the Fe-doped model was somehow different from the pure model, especially in the variation of coronene surface from planar mode to nonplanar mode in the Fe-doped region. Stabilization of H_2S with different starting positions at the surface yielded two conformational models of H_2S at the Fe-doped surface designated by H_2S-A and H_2S-B. All

starting positions almost reached these two models, as exhibited in Figure 1. Based on such structural optimization, IR spectra were evaluated (Figure 2) with no imaginary frequency to confirm the achieved minimized energy structures besides variations in signaling for the models. For the detection of H_2S adsorption at the Fe-doped coronene, recording IR spectra could help by analyzing the obtained results and those of references. Further analyses of the models were done by obtained values of bond lengths as exhibited in Figure 3, in which changes of structural geometries due to doping and adsorption were obvious for the models. Based on such results, it could be expected that electronic features would detect significant effects of structural variations, as shown by comparing the results of models. One important point is that the doped atom should only slightly change the structure, in which the results of bond lengths indicated that the most significant changes were seen for the bonds of the Fe-doped region without any significant effects for the bonds of other atomic regions. After H_2S adsorption, some new variations were observed for the bonds due to adding an external substance to the model. For interacting substances, two lengths of Fe-S interactions were found as 2.354 and 2.343 Å for H_2S-A and H_2S-B models. Although bond length is important for evaluating bind energies, other structural features of both adsorbent and adsorbed substances determine the strength of such complex formation. Evaluated Mulliken charge points (Figure 4) could help for a brighter description of model systems using more precise parameters. In this regard, such charge points could show higher/lower electron densities for the model systems to participate in interaction processes with other substances. Comparing pure and Fe-doped models could indicate that variations of +/– charge points were seen more reasonable for the Fe-doped model by locating + and – point charges besides each other in contrast with all + or all – regions for the pure model. This result could show the importance of atomic-doped models for tuning nanostructure properties to show specified features [11]. For the investigated model, the positive charge point of the Fe atom was ready to interact with a negative substance such as the S atom of H_2S. Because of such charge points, hydrogen atoms of H_2S were not relaxed toward the surface; they were located somehow parallel to the surface with a significant role of the S atom. Indeed, such a hypothesis of perpendicular conformational relaxation of H_2S at the Fe-doped surface was refused, whereas that of parallel relaxation was observed for the adsorbed models.

Table 1. Evaluated quantities for the optimized models.

Feature	Pure Coronene	Fe-Doped	H_2S-A	H_2S-B
E eV	-25078.082	-58420.955	-69289.506	-69289.498
Eads eV	n/a	n/a	-1.457	-1.449
BSSE eV	n/a	n/a	0.169	0.173
Fe-S Length Å	n/a	n/a	2.354	2.343
LUMO eV	0.181	-0.708	0.167	0.171
HOMO eV	-7.184	-6.739	-6.505	-6.488
EG eV	7.365	6.031	6.672	6.659
FE eV	-3.502	-3.724	-3.169	-3.158
DM Debye	0	0.815	4.342	4.511
V cm^3/mol	198.662	218.267	257.455	249.933
Qcc Fe MHz	n/a	44.701	53.779	51.547
Qcc S MHz	n/a	n/a	35.026	35.329

Results of obtained values of energies for the models were summarized in Table 1, indicating various types of energies for structure, binding, and molecular orbitals. In this regard, comparing energies for H_2S-A and H_2S-B models could indicate slightly better stability

for the A model with a supportive value of more negative binding energy. Although the length of Fe-S was shorter for the H_2S-B model, the H_2S-A model has seen a better choice of complex formation because of better localization of H_2S exactly at the Fe-doped region with centric S atom. The obtained values of BSSE were almost negligible, not changing the direction of obtained results. Further analyses of quantities for molecular orbital energies could indicate the impact of dopant and adsorbed substances on the electronic properties of structures. For the Fe atom, the existence of vacant orbitals might help the model for adsorbing electrons through the interaction process. In this regard, LUMO of the Fe-doped model was shifted to a lower level due to doping yielding a proper surface for adsorbing electron-rich S atom. Furthermore, the energy difference of HOMO and LUMO levels (EG) was also reduced for the Fe-doped model, making it a more reactive surface than pure coronene and supporting energy values of Fermi levels (FE). Although both H_2S-A and H_2S-B models were identical in several atoms, their conformational changes indicate that the electronic environment could lead to different complex models. In this case, EG's different values could help recognize each of adsorbed models based on the sensor function of the adsorbent nanosurface besides total sensing of the H_2S adsorption process at the Fe-doped surface.

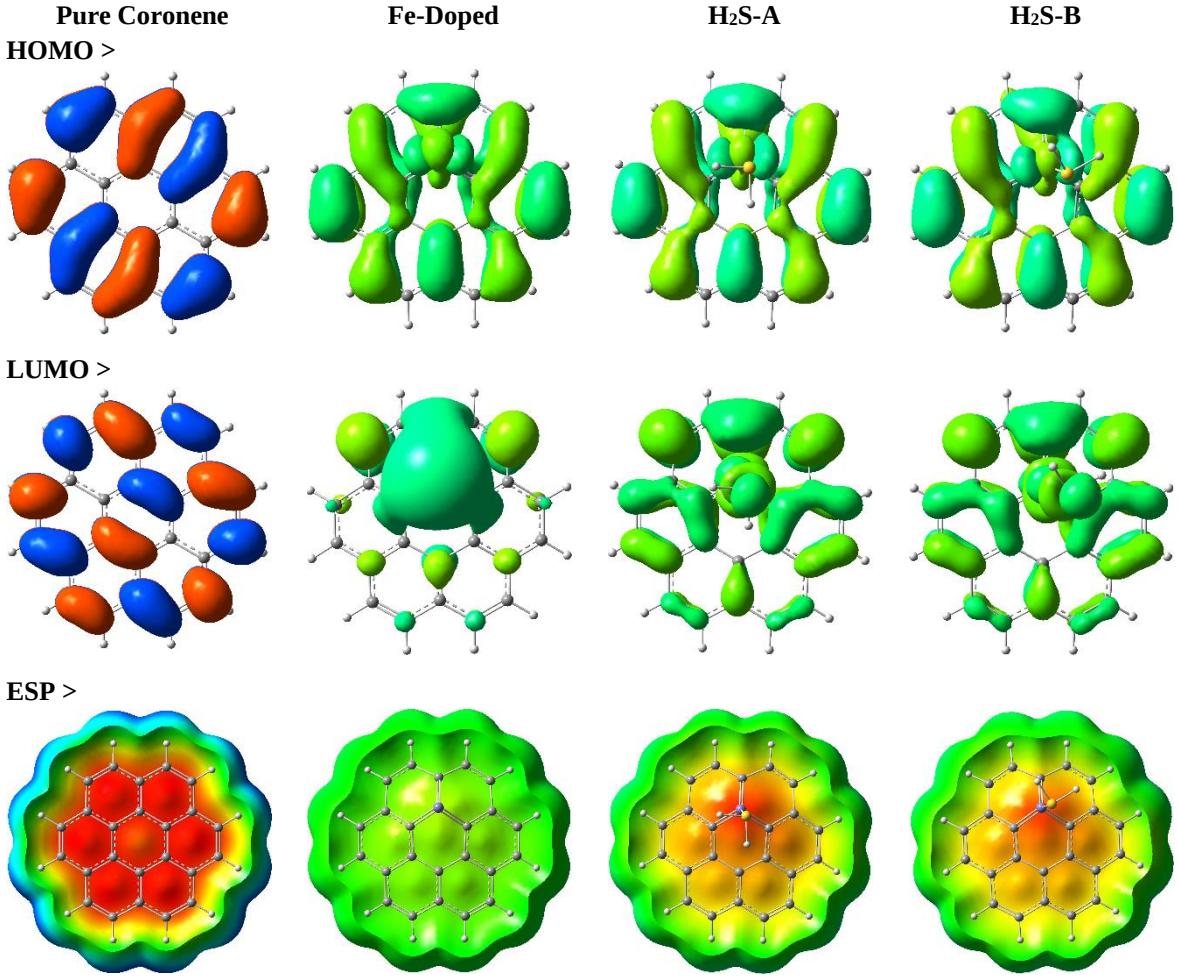

Figure 5. HOMO and LUMO distribution patterns and ESP surfaces for the optimized models. Red is in the negative, and Blue is in the positive direction with green in the middle.

Based on representations of HOMO and LUMO distribution patterns and ESP surfaces (Figure 5), such achievements of molecular orbitals features and dipole moment (DM) could be analyzed better. As indicated by the zero-value of DM for pure coronene, all HOMO and

LUMO distribution patterns and ESP were directly neutralizing each other, whereas those of other modes were almost in a better surface mode for interactions with higher values of DM. As indicated by energies for better stability of H_2S-A model than B model, lower value of DM was obtained for the first model indicating its stability regarding electric charge distribution slightly more than B model. Interestingly, the wider value of EG for the H_2S-A model than the B model also approved such better stability of the A model compared to the B model. The size of the volume (V) for the A model was also expanded more than the B model showing more relaxation status for the H_2S-A model. All such molecular-based features helped the discussion to distinguish structural stabilities and features for the model systems. More precise results were achieved by the obtained values of quadrupole coupling constants (Qcc) as useful tools for describing the electronic environment of materials at the atomic scale [33-35]. It was mentioned that the vacant orbitals of Fe were expected to work for electron hiring during the adsorption process from electron-rich S atom. In this regard, Qcc of Fe for the H_2S-A model was calculated in a higher field than that of the B model showing a better possibility of Fe-S interaction of the A model than the B model. It was known that the H_2S-A model was slightly more stable than the H_2S-B model by the obtained structural energies, in which such results were supported by a higher value of Qcc for Fe atom of A model than the B model making possible stronger binding mode. It is worth noting that only interacting distances are not enough for making decisions about interaction modes. The results of this work indicated the importance of electronic features, and even the orientation of adsorbed substances could yield distinguishing results for the models. Consequently, the Fe-doped coronene model could work for H_2S gas adsorption with precise descriptive details provided by this work at the molecular and atomic scales showing the benefit of employing such an adsorbent molecular system for the adsorption process.

4. Conclusions

This work was performed to investigate details of adsorption of H_2S gaseous substance at the Fe-doped coronene surface. To achieve this purpose, DFT calculations were performed to stabilize each of the pure and Fe-doped coronene models, then investigate H_2S adsorption processes in the complex formation of adsorbed gas at the surface. The first obtained results indicated that the Fe-doped model could provide a better surface than the pure model for participating in the adsorption process. Such achievement was supported by further analyses of the results for adsorption processes, which approved proper adsorption of H_2S gaseous substance at the Fe-doped surface. Examining different starting positions for H_2S molecule as the Fe-doped coronene surface yielded two models of H_2S-A and H_2S-B models of adsorbed gas at the surface with different properties. Based on values of energies for structures and binding process, the H2S-A model was seen in a better mode of stability than the H_2S-B model. Other obtained results for energy levels of molecular orbitals also indicated better stability for the H2S-A model than the H_2S-B model. Besides all quantities, visual representations of models also described details of H_2S adsorption at the Fe-doped surface. Atomic-scale properties indicated that the Fe atom of the H_2S-A model could hire more electrons from the S atom in comparison with the H_2S-B model resulting in stronger binding for the A model. Consequently, the Fe-doped model of coronene was seen suitable for adsorbing H_2S substance with detailed information making possible the diagnosis of such gas adsorption in addition to removal purposes of environmental health care systems.

Funding

This research received no external funding.

Acknowledgments

This research has no acknowledgment.

Conflicts of Interest

The authors declare no conflict of interest.

References

1. Iijima, S. Carbon nanotubes: past, present, and future. *Physica B* **2020,** *323*, 1-5, https://doi.org/10.1016/S0921-4526(02)00869-4.
2. Mirzaei, M. Nanotechnology for science and engineering. *Advanced Journal of Science and Engineering* **2020,** *1*, 67-68, https://doi.org/10.22034/AJSE2013067.
3. Mirzaei, M. Calculation of chemical shielding in C-doped zigzag BN nanotubes. *Monatshefte für Chemie* **2009,** *140*, 1275-1279, https://doi.org/10.1007/s00706-009-0195-6.
4. Harismah, K.; Mirzaei, M.; Da'I, M.; Roshandel, Z.; Salarrezaei, E. In silico investigation of nanocarbon biosensors for diagnosis of COVID-19. *Eurasian Chemical Communications* **2021,** *3*, 95-102, https://doi.org/10.22034/ecc.2021.267226.1120.
5. Tang, Z.; Zhang, X.; Shu, Y.; Guo, M.; Zhang, H.; Tao, W. Insights from nanotechnology in COVID-19 treatment. *Nano Today* **2021,** *36*, 101019, https://doi.org/10.1016/j.nantod.2020.101019.
6. Brunner, M.; Imberti, S.; Simmons, B.A.; Warr, G.G.; Atkin, R. Liquid nanostructure of cholinium argininate biomass solvents. *ACS Sustainable Chemistry & Engineering* **2021,** *9*, 2880-2890, https://doi.org/10.1021/acssuschemeng.0c08829.
7. Zumpano, R.; Polli, F.; D'Agostino, C.; Antiochia, R.; Favero, G.; Mazzei, F. Nanostructure-based electrochemical immunosensors as diagnostic tools. *Electrochem* **2021,** *2*, 10-28, https://doi.org/10.3390/electrochem2010002.
8. Sherafati, M.; Rad, A.S.; Ardjmand, M.; Heydarinasab, A.; Peyravi, M.; Mirzaei, M. Beryllium oxide (BeO) nanotube provides excellent surface towards adenine adsorption: a dispersion-corrected DFT study in gas and water phases. *Current Applied Physics* **2018**, *18*, 1059-1065, https://doi.org/10.1016/j.cap.2018.05.024.
9. Mirzaei, M.; Mirzaei, M. Sulfur doping at the tips of (6, 0) boron nitride nanotube: a DFT study. *Physica E* **2010,** *42*, 2147-2150, https://doi.org/10.1016/j.physe.2010.04.014.
10. Jalali Sarvestani, M.R.; Ahmadi, R. Adsorption of TNT on the surface of pristine and N-doped carbon nanocone: a theoretical study. *Asian Journal of Nanosciences and Materials* **2020,** *3*, 103-114, https://doi.org/10.26655/AJNANOMAT.2020.2.2.
11. Mirzaei, M.; Mirzaei, M. The C-doped AlP nanotubes: a computational study. *Solid State Sciences* **2011,** *13*, 244-250, https://doi.org/10.1016/j.solidstatesciences.2010.11.022.
12. Salamanca-Buentello, F.; Daar, A.S. Nanotechnology, equity and global health. *Nature Nanotechnology* **2021,** *16*, 358-361, https://doi.org/10.1038/s41565-021-00899-z.
13. Moreno-Lanceta, A.; Medrano-Bosch, M.; Melgar-Lesmes, P. Single-walled carbon nanohorns as promising nanotube-derived delivery systems to treat cancer. *Pharmaceutics* **2020,** *12*, 850, https://doi.org/10.3390/pharmaceutics12090850.
14. Rad, A.S.; Mirabi, A.; Peyravi, M.; Mirzaei, M. Nickel-decorated B12P12 nanoclusters as a strong adsorbent for SO2 adsorption: quantum chemical calculations. *Canadian Journal of Physics* **2017,** *95*, 958-962, https://doi.org/10.1139/cjp-2017-0119.
15. Kakaei, A.; Mirzaei, M. Cyclophosphamide@ CNT: in silico exploration of nano drug delivery system. *Lab-in-Silico* **2021,** *2*, 9-14, https://doi.org/10.22034/labinsilico21021009.
16. Saini, V.; Chinta, K.C.; Reddy, V.P.; Glasgow, J.N.; Stein, A.; Lamprecht, D.A.; Rahman, M.A.; Mackenzie, J.S.; Truebody, B.E.; Adamson, J.H.; Kunota, T.T. Hydrogen sulfide stimulates Mycobacterium tuberculosis respiration, growth and pathogenesis. *Nature Communications* **2020,** *11*, 1-17, https://doi.org/10.1038/s41467-019-14132-y.

17. Paul, B.D.; Snyder, S.H.; Kashfi, K. Effects of hydrogen sulfide on mitochondrial function and cellular bioenergetics. *Redox Biology* **2021,** *38*, 101772, https://doi.org/10.1016/j.redox.2020.101772.
18. Szabo, C. Hydrogen sulfide, an endogenous stimulator of mitochondrial function in cancer cells. *Cells* **2021,** *10*, 220, https://doi.org/10.3390/cells10020220.
19. Khoma, M.S.; Ivashkiv, V.R.; Chuchman, M.R.; Vasyliv, C.B.; Ratska, N.B.; Datsko, B.M. Corrosion cracking of carbon steels of different structure in the hydrogen sulfide environment under static load. *Procedia Structural Integrity* **2018,** *13*, 2184-2189, https://doi.org/10.1016/j.prostr.2018.12.143.
20. Georgiadis, A.G.; Charisiou, N.D.; Goula, M.A. Removal of hydrogen sulfide from various industrial gases: a review of the most promising adsorbing materials. *Catalysts* **2020,** *10*, 521, https://doi.org/10.3390/catal10050521.
21. Wang, Y.; Wang, Y.; Liu, Y. Removal of gaseous hydrogen sulfide using ultraviolet/Oxone-induced oxidation scrubbing system. *Chemical Engineering Journal* **2020,** *393*, 124740, https://doi.org/10.1016/j.cej.2020.124740.
22. Kailasa, S.K.; Koduru, J.R.; Vikrant, K.; Tsang, Y.F.; Singhal, R.K.; Hussain, C.M.; Kim, K.H. Recent progress on solution and materials chemistry for the removal of hydrogen sulfide from various gas plants. Journal of Molecular Liquids **2020,** *297*, 111886, https://doi.org/10.1016/j.molliq.2019.111886.
23. Fawcett, E.; Trotter, J. The crystal and molecular structure of coronene. *Proceedings of the Royal Society of London* **1966,** *289*, 366-376, https://doi.org/10.1098/rspa.1966.0017.
24. Harismah, K.; Mirzaei, M.; Moradi, R. DFT studies of single lithium adsorption on coronene. *Zeitschrift für Naturforschung A* **2018,** *73*, 685-691, https://doi.org/10.1515/zna-2017-0458.
25. Moezi, E.; Mirzaei, M. Graphene scaffold for tioguanine delivery: DFT approach. *Lab-in-Silico*, **2021,** *2*, 25-29, https://doi.org/10.22034/labinsilico21021025.
26. Gupta, N.K.; Bae, J.; Kim, S.; Kim, K.S. Fabrication of Zn-MOF/ZnO nanocomposites for room temperature H2S removal: Adsorption, regeneration, and mechanism. *Chemosphere* **2021,** *274*, 129789, https://doi.org/10.1016/j.chemosphere.2021.129789.
27. Scheufele, F.B.; da Silva, E.S.; Cazula, B.B.; Marins, D.S.; Sequinel, R.; Borba, C.E.; Patuzzo, G.S.; Lopez, T.F.M.; Alves, H.J. Mathematical modeling of low-pressure H2S adsorption by babassu biochar in fixed bed column. *Journal of Environmental Chemical Engineering* **2021,** *9*, 105042, https://doi.org/10.1016/j.jece.2021.105042.
28. Rad, A.S.; Aghaei, S.M.; Pazoki, H.; Binaeian, E.; Mirzaei, M. Surface interaction of H2O and H2S onto Ca12O12 nanocluster: quantum-chemical analyses. *Surface and Interface Analysis* **2018,** *50*, 411-419, https://doi.org/10.1002/sia.6382.
29. McArdle, S.; Endo, S.; Aspuru-Guzik, A.; Benjamin, S.C.; Yuan, X. Quantum computational chemistry. *Reviews of Modern Physics* **2020,** *92*, 015003, https://doi.org/10.1103/RevModPhys.92.015003.
30. Mirzaei, M. Making sense the ideas in silico. *Lab-in-Silico* **2020,** *1*, 31-32, https://doi.org/10.22034/lins20012031.
31. Pence, H.E.; Williams, A. ChemSpider: an online chemical information resource. *Journal of Chemical Education* **2010,** *87*, 1123-1124, https://doi.org/10.1021/ed100697w.
32. Frisch, M.; Trucks, G.; Schlegel, H.; Scuseria, G.; Robb, M.; Cheeseman, J.; Montgomery Jr, J.; Vreven, T.; Kudin, K.; Burant, J. Gaussian 09 D.01 Program. Gaussian. Inc.: Wallingford, CT, USA. **2009**.
33. Seif, A.; Mirzaei, M.; Aghaie, M.; Boshra, A. AlN nanotubes: a DFT study of Al-27 and N-14 electric field gradient tensors. *Zeitschrift für Naturforschung A* **2007,** *62*, 711-715, https://doi.org/10.1515/zna-2007-1206.
34. Mirzaei, M.; Yousefi, M. Computational studies of the purine-functionalized graphene sheets. *Superlattices and Microstructures* **2012,** *52*, 612-617, https://doi.org/10.1016/j.spmi.2012.06.027.
35. Mirzaei, M.; Hadipour, N.L. Density functional calculations of 14N and 11B NQR parameters in the H-capped (6, 0) and (4, 4) single-walled BN nanotubes. *Physica E* **2008,** *40*, 800-804, https://doi.org/10.1016/j.physe.2007.10.050.